Journal of Inflammation Research Dovepress

Open Access Full Text Article ORIGINAL RESEARCH

Cardamonin Attenuates Myocardial Ischemia/Reperfusion-Induced Ferroptosis Through Promoting STAT3 Signaling

Tao Yang[1,2,*], Pengcui Wu[2,*], Luping Jiang[2], Ran Chen[2], Qiao Jin[2], Guohong Ye[2]

[1]Department of Cardiovascular Medicine, The Second Affiliated Hospital, School of Medicine, The Chinese University of Hong Kong, Shenzhen & Longgang District People's Hospital of Shenzhen, Guangdong, 518172, People's Republic of China; [2]Department of Cardiovascular Medicine, The Affiliated Changsha Central Hospital, Hengyang Medical School, University of South China, Changsha, 410004, People's Republic of China

*These authors contributed equally to this work

Correspondence: Guohong Ye; Qiao Jin, Department of Cardiovascular Medicine, The Affiliated Changsha Central Hospital, Hengyang Medical School, University of South China, No. 161 Shaoshan South Road, Changsha, 410004, People's Republic of China, Email ygh120811@163.com; jinqiaonhdx@163.com

Objective: Ferroptosis is intricately associated with the pathophysiology processes of myocardial ischemia. Cardamonin (CAR) has been shown to provide significant protection against tissue damage due to multiple ischemia/reperfusion. This study aimed to examine the cardioprotective properties of CAR in myocardial ischemia/reperfusion injury (MIRI) and provide insights into the possible mechanisms involved.

Methods: An MIRI mice model was conducted by coronary artery ligation, and the effects of CAR on myocardial tissue damage were evaluated by infarct size assessment, echocardiography, and H&E staining. The extent of ferroptosis was detected by examining the levels of ferroptosis-related proteins and lipid reactive oxygen species (ROS). The function pathway of CAR was analyzed by network pharmacology and verified using Western blotting. In addition, we induced hypoxia/reoxygenation (H/R) in cardiomyocytes to detect SLC7A11 expression, ROS level, mitochondrial iron content, and oxidative stress marker levels. The target protein of CAR was identified by Western blotting and molecular docking. We then evaluated the regulatory role of STAT3 on MIRI-induced ferroptosis by silencing STAT3.

Results: In our study, CAR demonstrated a reduction in myocardial histopathological damage and mitigation of ferroptosis in MIRI mice. Through network pharmacology analysis and Western blotting, our findings indicated that CAR modulates the AGE-RAGE signaling pathway, particularly impacting STAT3. Meanwhile, in vitro experiments revealed that advanced-glycation end products (AGEs) exacerbated H/R-induced ferroptosis, whereas CAR alleviated this ferroptosis in the presence of both AGEs and H/R. CAR was observed to enhance STAT3 expression in H/R+AGRs-treated cardiomyocytes. Molecular docking results demonstrated favorable binding interactions between CAR and STAT3. Our study confirmed that CAR mitigated MIRI-induced myocardial injury and ferroptosis through targeting STAT3 in mice.

Conclusion: In conclusion, CAR inhibited ferroptosis by activating the STAT3 signaling, thereby mitigating MIRI.

Keywords: cardamonin, myocardial ischemia/reperfusion injury, ferroptosis, STAT3, AGE-RAGE signaling pathway

Introduction

Myocardial infarction (MI) is a significant cause of death worldwide.[1,2] Timely reperfusion is crucial in medical practice for salvaging ischemic myocardial tissue, reducing infarct size, preserving left ventricular systolic function, and preventing heart failure. However, reperfusion therapy can paradoxically result in myocardial injury and exacerbate cardiac function, known as myocardial ischemia/reperfusion injury (MIRI).[3] Research has shown that reperfusion injury contributes to about half of the total myocardial infarction area.[4] The mechanisms underlying MIRI are complex and involve processes such as necroptosis, apoptosis, autophagy, pyroptosis, disruptions in energy metabolism, intracellular

Received: 10 July 2024
Accepted: 31 October 2024
Published: 15 November 2024

calcium overload, cellular inflammation, and oxidative stress.[5–8] Given the limited efficacy of various strategies in mitigating ischemic myocardial infarction and dysfunction in animal models and clinical settings, alternative mechanisms warrant further investigation.

Ferroptosis is a newly recognized type of programmed cell death distinguished by an accumulation of intracellular iron, reduction of glutathione levels, and lipid peroxidation.[9,10] This mechanism has been associated with the pathogenesis of several cardiovascular disorders, such as MIRI.[11,12] Increasing evidence suggests that ferroptosis is the main mode of cardiomyocyte death in MIRI.[9] Fang et al first demonstrated that during ischemia/reperfusion, degradation of ferritin releases iron, which triggers the iron-mediated Fenton reaction in mitochondria, leading to lipid peroxidation and subsequent cardiac injury.[13] A follow-up study by Hiroyuki Tsutsui et al demonstrated that hypoxia/reoxygenation increases heme oxygenase 1 levels and induces iron overload in the endoplasmic reticulum, which promotes the overproduction of lipid peroxidation and subsequent ferroptosis in cardiomyocytes.[14] Additionally, cardiomyocyte ferroptosis exacerbates MIRI.[15,16] Ferroptosis inhibitors reduced infarct size and attenuated myocardial fibrosis in a mouse model of MIRI.[17] Targeted ferroptosis also protects the heart from I/R-induced myocardial remodeling and heart failure.[18,19] Consequently, targeting ferroptosis for reduction presents a promising approach to mitigate myocardial injury.

Cardamonin (CAR), originating from the Zingiberaceae botanical family, has garnered interest due to its diverse range of properties, notably its antioxidant, anti-inflammatory, and antiapoptotic effects.[20] Studies have indicated that CAR exhibits protective characteristics by modulating various signaling pathways implicated in a variety of medical conditions including cancer, diabetes, cardiovascular diseases, and inflammatory disorders.[21,22] In a variety of ischemia/reperfusion (I/R)-induced tissue injuries, CAR mitigates the injuries by modulating oxidative stress and inflammation.[23–25] In heart disease, CAR also prevents Adriamycin-induced cardiotoxicity,[26] lipopolysaccharide-induced myocardial contractile dysfunction,[27] and transverse aortic constriction (TAC)-induced myocardial hypertrophy[28] in mice. In addition, CAR inhibits ferroptosis by modulating downstream signaling pathways, thereby attenuating cellular inflammation.[29] However, the specific regulatory pathways of CAR in attenuating ferroptosis are still unclear, including the targets of CAR action and its downstream regulatory pathways. These still need to be further explored.

In this study, we assessed the effects of CAR on ferroptosis in cardiomyocytes treated with hypoxia/reoxygenation (H/R) and MIRI mice. Our study offers important insights into ferroptosis in MIRI and highlights a potential target for MIRI treatment.

Materials and Methods

Animal and Ethics Statement

Healthy adult male C57BL/6 mice (8 weeks) were procured from Hunan SJA Laboratory Animal Co., Ltd, China. The animals were housed in a controlled environment with a temperature range of 20°C-25°C, humidity maintained at 40%-50%, and subjected to a standard light-dark cycle. All experimental protocols were conducted in compliance with the relevant guidelines. The study obtained approval from the Medical Ethics Committee of the University of South China.

Establishment of Mouse MIRI Model and Grouping

As described previously,[14,30] mice were anesthetized with sodium pentobarbital (60 mg/kg i.p), the intercostal space was opened under mechanical ventilation and myocardial ischemia was induced by ligation of the anterior descending branch of the left coronary artery (LAD) for 45 min, followed by reperfusion for 4 h. In the sham-operated (Sham) group, the LAD was not ligated with sutures. Blood was collected before MIRI and mice were eliminated from the study if they exhibited elevated levels of cardiac dysfunction markers such as LDH and CK-MB. Mice in the CAR intervention group received CAR treatment (B7085, APExBIO, Houston, USA; 20 mg/kg, P.O. orally[27]) 1 h before perfusion. After 4 h of reperfusion,[30] echocardiography was performed to record left ventricular ejection fraction (LVEF) and left ventricular internal diastolic diameter (LVIDd) in mice. Mice were executed by cervical dislocation, hearts were then excised, and infarct size was measured.

In order to investigate the impact of CAR on MIRI, mice were divided into four groups through random allocation: Sham, Sham+CAR, I/R, and I/R+CAR. Furthermore, to investigate the impact of signal transducer and activator of transcription 3 (STAT3) on MIRI, additional mice were divided into five groups: Sham, I/R, I/R+CAR, I/R+CAR+sh-NC, and I/R+CAR+sh-STAT3. Anesthetized mice were intubated and ventilated using an HX-300S animal ventilator for intracoronary administration of adenoviruses. The heart was accessed via a minor left anterior thoracotomy, and adenoviruses containing sh-NC, sh-STAT3 were injected into the aortic root from the left ventricular apex using a catheter, while the aorta and pulmonary arteries were temporarily clamped for 20 sec.[30] After removing air and blood and closure of the chest, the mice were allowed to recuperate. Subsequently, five days' post-adenovirus injection, the mice underwent I/R treatment.

Infarct Size Assessment

Following reperfusion, the assessment of myocardial infarct size[30] was conducted by re-occluding the LAD and administering Evans blue dye (AWI0511, Abiowell, Changsha, China; 1 mL of 2% solution via the jugular vein) to outline the ischemic region. Subsequently, mice were subjected to euthanasia, and their hearts were promptly removed and sliced. The heart sections were then exposed to 1.0% TTC at 37°C for 15 min to distinguish between viable myocardium (red) and necrotic or infarcted myocardium (white). Following rinsing with cold sterile saline, the sections were fixed in 10% formaldehyde, weighed, and imaged from both aspects. The determination of infarcted areas (INF) and areas at risk was carried out utilizing computer-assisted area measurement. The infarct area relative to the left ventricle (INF/LV, %) and the infarct area as a percentage of the at-risk area were subsequently calculated.

Hematoxylin-Eosin (HE) Staining

Cardiac samples were fixed using a 4% paraformaldehyde solution (AWI0056b, Abiowell), embedded in paraffin, and sectioned into 5 μm slices. Subsequently, the slices were mounted on slides for hematoxylin staining for 1–10 min and eosin staining for 1–5 min, which were then examined using an optical microscope (BA210T, Motic, Xiamen, China).

Western Blotting

The cell and tissue samples were lysed using RIPA buffer (AWB0136, Abiowell) supplemented with 1% phenylmethanesulfonyl fluoride (AWH0642, Abiowell). The concentration of total proteins was determined using a BCA protein assay kit (AWB0104, Abiowell). Following electrophoresis, the proteins were subsequently transferred onto polyvinylidene fluoride membranes. In order to prevent non-specific binding of antibodies, these membranes were subsequently blocked with 5% skim milk at room temperature while being agitated on a shaker. Subsequently, the proteins were subjected to incubation with primary antibodies targeting GPx4 (1: 1000; 30388-1-AP, ProteinTech Group, Chicago, IL, USA), SLC7A11 (1: 1000; AWA57291, Abiowell), AKT1 (1: 2000; AWA02183, Abiowell), JUN (1: 5000; 66313-1-Ig, ProteinTech Group), MMP2 (1: 800; 10373-2-AP, ProteinTech Group), NFKB1 (1: 1000; AWA44182, Abiowell), STAT3 (1: 10000; 10253-2-AP, ProteinTech Group), TNF (1: 2000; 60291-1-Ig, ProteinTech Group), and advanced-glycation end products (AGEs, 1: 2000; Bs-1158R, Bioss, Beijing, China) overnight at 4°C. Subsequently, the specimens underwent a washing procedure and were subsequently exposed to the secondary antibody, HRP goat anti-mouse IgG (1: 5000; AWS0001, Abiowell) and HRP goat anti-rabbit IgG (1: 5000; AWS0002, Abiowell), at ambient temperature for a duration of 1 h. Following an additional washing step, the membranes were subjected to visualization using an ECL chemiluminescence detection kit (AWB0005, Abiowell). The internal reference protein was GAPDH (1: 5000; AWA80009, Abiowell).

Lipid Reactive Oxygen Species (ROS) Determination

The lipid ROS level was evaluated using C11-BODIPY 581/591 (HY-D1301, MedChem Express, Monmouth Junction, NJ, USA) in accordance with established protocol.[31] In summary, cells were trypsinized, resuspended in 400 μL of serum-free medium containing BODIPYTM 581/591 C11 (10 μM), and incubated at 37 °C for 30 min in a cell culture incubator. Subsequently, fluorescence emission peaks were assessed using a flow cytometer (A00-1-1102, Beckman Coulter, Brea, CA, SA).

Immunofluorescence (IF) Analysis

The tissue specimens were gathered and subjected to IF analysis. Initially, the samples were treated with 4% paraformaldehyde for fixation, followed by permeabilization using 0.3% Triton X-100 (AWB0141, Abiowell) and subsequently blocked with 5% BSA (AW10127b, Abiowell) for 30 min. Following this, the samples were exposed to primary antibodies against SLC7A11 (1:100; 26864-1-AP, ProteinTech Group) and Troponin T (1:100; 68300-1-Ig, ProteinTech Group) overnight at 4°C. Subsequent to the primary antibody incubation, the samples were treated with secondary antibodies, specifically goat anti-mouse antibody labeled with CoraLite488 (SA00013-1, ProteinTech Group) and goat anti-rabbit antibody labeled with CoraLite594 (SA00013-4, ProteinTech Group) for an additional 30 min at 37°C. Finally, the samples were stained with DAPI (AWC0291a, Abiowell) for 10–20 min, and imaging was performed using a confocal laser scanning microscope (BA410T, Motic).

Network Pharmacology Construction

Component Target Finding

First of all, the Simplified Molecular-Input Line-Entry System (SMILES) identifier of CAR was obtained from the PubChem database (https://pubchem.ncbi.nlm.nih.gov/) and subsequently imported into the Swiss Target Prediction database (http://www.swisstargetprediction.ch/) and Similarity ensemble approach (SEA) database (http://sea.bkslab.org/) to retrieve the corresponding component targets, and component targets with a likelihood score > 0 were considered for inclusion. All targets were rectified using the UniProt database (https://www.uniprot.org/) to eliminate non-human targets.

Disease Target Finding

Human gene searches were performed in the GeneCards database (https://www.genecards.org/) and NCBI gene database (https://www.ncbi.nlm.nih.gov/) using "Myocardial ischemia-reperfusion injury" and "ferroptosis" as the keywords on September 24, 2023. After combining the genes from these two databases, disease-related genes were obtained. The screened CAR targets were subjected to Venn diagramming with the disease targets.

Kyoto Encyclopedia of Genes and Genomes (KEGG) Enrichment

The shared targets between the CAR, MIRI, and ferroptosis were found to be enriched for KEGG pathways. *P.* adjust < 0.05 was the screening criterion. Bubble plots and histograms were generated by utilizing the clusterProfiler package in R 4.0.3.

Isolation and Extraction of Primary Mouse Cardiomyocytes

Neonatal murine cardiac myocytes (NMCM) were obtained from newborn C57BL/6 mice aged 1–2 days, following established protocols.[14,30] In brief, the mice were anesthetized with sodium pentobarbital and sterilized by total body immersion in 75% alcohol for 3 min. The hearts were exposed and were gently squeezed with forceps to drain blood remaining in the heart chambers. Ophthalmic scissors were used to carefully snip the heart tissue, which was washed by adding pre-cooled PBS buffer. Subsequently, 5 mL of 0.08% trypsin was added for initial digestion at 37°C for 6 min and the first supernatant was discarded. Further digestion was performed by adding 5 mL of 0.125% collagenase II for 6 min at 37°C on a shaker. The remaining myocardial tissue was then re-digested by adding 5 mL of 0.125% collagenase II and filtered to obtain cardiomyocytes. The cells were then suspended in coated medium and subjected to cell survival and iron content assays. The experiments were conducted within a limited number of passages to ensure cell viability and consistency in results.

Cell Culture and Hypoxia/Reoxygenation (H/R) Model

NMCM and HL-1 cells (AW-CNM080, Abiowell) were cultured in MEM medium (AW-M001, Abiowell) supplemented with 10% fetal bovine serum (FBS; AWC0219a, Abiowell) and 1% penicillin-streptomycin solution (AWH0529a, Abiowell). The cells were maintained in a humidified atmosphere containing 5% CO_2 at 37°C. The culture media were refreshed every 2 days, and prior to treatments, the cells were exposed to a serum-free medium for 12 h. To establish the H/R model,[32] cells were cultured in a hypoxic environment (1% O_2+5% CO_2+94% N_2) in sugar-free serum-

free medium for 3 h to induce hypoxic conditions. Following this, the cells were re-oxygenated by replacing the buffer with normal medium containing serum and exposing them to normal oxygen levels for 2 h.

Cell Transfection

STAT3-specific shRNA molecules (HG-SM139276, Honorgene) were synthesized chemically by HonorGene Company (Changsha, China). A non-specific shRNA (scramble) containing a non-target sequence was used as a control. Transfection was carried out using 3 μg shRNA plasmids and 5 μL Lip2000 reagent (11668019, Invitrogen, Carlsbad, CA, USA). Following the silencing of STAT3, cells were given a 48-h period in fresh growth medium. The effectiveness of transfection was evaluated through Western blotting. Following this assessment, the cells were treated with CAR for 1 h after the 48-h transfection period and then exposed to H/R.

Cell Treatments

Prior to the H/R intervention, different concentrations of AGEs (5, 50, 100, 150, 200 μg/mL;[33,34] 22968–10, Cayman Chemical Co., Ann Arbor, MI) or BSA (as a control for the AGEs; Sigma-Aldrich) were exposed for 24 h.[34] To evaluate the effect of CAR on H/R-induced cardiomyocyte injury, cells were subjected to CAR (10 μmol/L[27]) interventions prior to 1 h of H/R induction. To assess the involvement of ferroptosis in the modulatory role of AGEs or CAR on H/R-induced cardiomyocyte injury, Fer-1 (ferroptosis inhibitor, 50 μmol/L;[14] HY-100579, MedChem Express, Monmouth Junction, NJ, USA) was performed 1 h prior to H/R induction.

Cell Viability Assay

Cell viability was evaluated through a CCK-8 assay kit (AWC0114, Abiowell) following the instructions provided by the manufacturer. Specifically, 5000 cells were seeded in 100 μL of growth medium in a 96-well plate. Subsequently, 10 μL of CCK-8 solution was introduced into each well during the final stage of treatment, followed by a 4-h incubation at 37°C. Optical density (OD) values at 450 nm were then measured using a microplate absorbance reader (MB-530, Heales, Shenzhen, China).

Detection of Mitochondrial Fe^{2+} and ROS

To evaluate the contents of mitochondrial Fe^{2+} and ROS, cells were supplemented with 5 μmol/L of Mito-FerroGreen (M489, Dojindo, Kumamoto, Japan) and 200 nmol/L of the mitochondrial staining probe MitoSox Red (40778ES50, Yeasen, Shanghai, China), respectively. Subsequently, cells were incubated in a CO_2 incubator for 30 min, the staining working solution was removed, and fresh cell cultures medium pre-warmed and incubated at 37°C were added, followed by observation by fluorescence microscopy.

Analysis of Antioxidants and Oxidative Stress Markers

The levels of glutathione (GSH), malondialdehyde (MDA), and superoxide dismutase (SOD) were analyzed using GSH Assay Kit (A006-2-1, Nanjing Jiancheng Bioengineering Institute, Nanjing, China), MDA Assay Kit (A003-1, Nanjing Jiancheng Bioengineering Institute), and SOD Assay Kit (A001-3, Nanjing Jiancheng Bioengineering Institute) by colorimetry, respectively.

Cell Death Assay

In order to assess cell death, propidium iodide (PI)-positive cell staining was quantified through the utilization of a flow cytometer (A00-1-1102, Beckman Coulter). Cells were subjected to serum-free DMEM to induce cell death. Subsequently, the cells were collected, stained with PI (C2015S-2, Beyotime, Shanghai, China) at a concentration of 50 μg/mL for 10 min at room temperature and in the dark, and analyzed using a flow cytometer.

Statistical Analysis

All data were presented as the mean ± standard deviation (SD). Statistical analyses were conducted using GraphPad Prism 8.0 (GraphPad Software Inc., San Diego, CA, USA). The *t*-test was employed to compare two groups, whereas

one-way analysis of variance (ANOVA) was utilized to compare multiple groups. $P < 0.05$ was considered statistically significant.

Results

CAR Intervention Alleviates MIRI-Induced Ferroptosis

Several studies have reported the ability of CAR to alleviate tissue damage caused by I/R.[23–25] To assess the protective impact of CAR on MIRI in mice, we conducted a mouse model of MIRI through coronary artery ligation followed by reperfusion. As displayed in Figure 1A, CAR treatment significantly restored MIRI-induced augment of infarct size. In addition, the administration of CAR led to a notable decrease in INF/LV ratio and enhancement in left ventricular function as indicated by LVEF and LVIDd measurements (Figure 1B-D). The degree of myocardial damage was assessed using HE staining. Figure 1E illustrates that the myocardial tissue structure of mice in the Sham group exhibited normal characteristics, devoid of edema, lesions, or neutrophil infiltration. Conversely, mice in the MIRI group displayed severe myocardial injury, evidenced by inflammation and interstitial edematous lesions within the myocardial tissue. Notably, the administration of CAR partially ameliorated the aforementioned pathological alterations. These findings indicate that CAR has the potential to mitigate structural modifications in the myocardium subsequent to I/R injury.

Furthermore, CAR has been found to inhibit ferroptosis by modulating downstream signaling pathways.[29] Ferroptosis is characterized by intracellular iron accumulation, reduced GSHlevels and lipid peroxidation. GPX4 is currently considered to be a central inhibitor of ferroptosis, and its activity is dependent on the production of GSH by activation of the cystine-glutamate reverse transporter protein, SLC7A11.[35] Therefore, we then explore the expression of ferroptosis-related proteins in MIRI mice. As expected, the levels of GPx4 and SLC7A11 were remarkably reduced, while they were restored when CAR administration (Figure 1F). Moreover, compared to the I/R group, the increased lipid ROS level induced by MIRI was significantly inhibited (Figure 1G). The number of SLC7A11-positive cells also decreased in the I/R-injured myocardium, which was significantly promoted after CAR treatment (Figure 1H). These results suggest that CAR could attenuate myocardial injury and ferroptosis to a certain degree.

Network Pharmacological Analysis of CAR-Regulated AGE-RAGE Signaling Pathway

To investigate the mechanisms of CAR in treating MIRI, we conducted network pharmacology. Initially, we collected MIRI- and ferroptosis-related targets from GeneCards and NCBI databases and CAR-related targets from the SEA and Swiss Target Prediction databases. After conducting a matching analysis between the 1226 MIRI-related targets, 2083 ferroptosis-related targets, and 274 CAR-related targets, we found 17 targets to be potential targets for CAR in treating MIRI (Figure 2A). To comprehend the functional pathways associated with the potential targets, we constructed a KEGG pathway enrichment analysis. Based on the findings of KEGG enrichment analysis, the "AGE-RAGE signaling pathway in diabetic complications" exhibited notable significance as indicated in Figure 2B. AGEs have been reported to accelerate I/R injury in cardiac microvascular endothelial cells.[36] In addition, AGE intervention stimulates ferroptosis.[33,34] Combined with Network pharmacological analysis, it can be hypothesized that CAR alleviates ferroptosis possibly through the AGE-RAGE signaling pathway. We then validated the expression of AGE-RAGE signaling pathway-related indicators in myocardial tissues. As depicted in Figure 2C, I/R treatment led to a notable elevation in levels of AGEs, NFKB1, TNF, JUN, and MMP2, alongside a significant reduction in AKT1 and STAT3. Notably, compared to the I/R group, CAR effectively inhibited the AGE expression level and promoted the expression of AKT1, NFKB1, STAT3, and TNF, while there was no significant difference in the expression of JUN and MMP2 after CAR treatment. Among them, the STAT3 showed the most significant difference. Above all, CAR might mitigate MIRI-induced ferroptosis through the AGE-RAGE signaling pathway.

AGEs Promote H/R-Induced Ferroptosis in Cardiomyocyte

Next, we investigated the effect of AGEs on cardiomyocyte ferroptosis in vitro. Primary mouse cardiomyocytes and HL-1 cells were treated with different concentrations of AGEs (5, 50, 100, 150, 200 μg/mL) and subjected to CCK-8 assay. The cell viability was unchanged when treated with 50–150 μg/mL AGEs, whereas 200 μg/mL AGEs induced acute toxicity (Figure 3A). Moreover, H/R intervention was performed after treating primary cardiomyocytes and HL-1

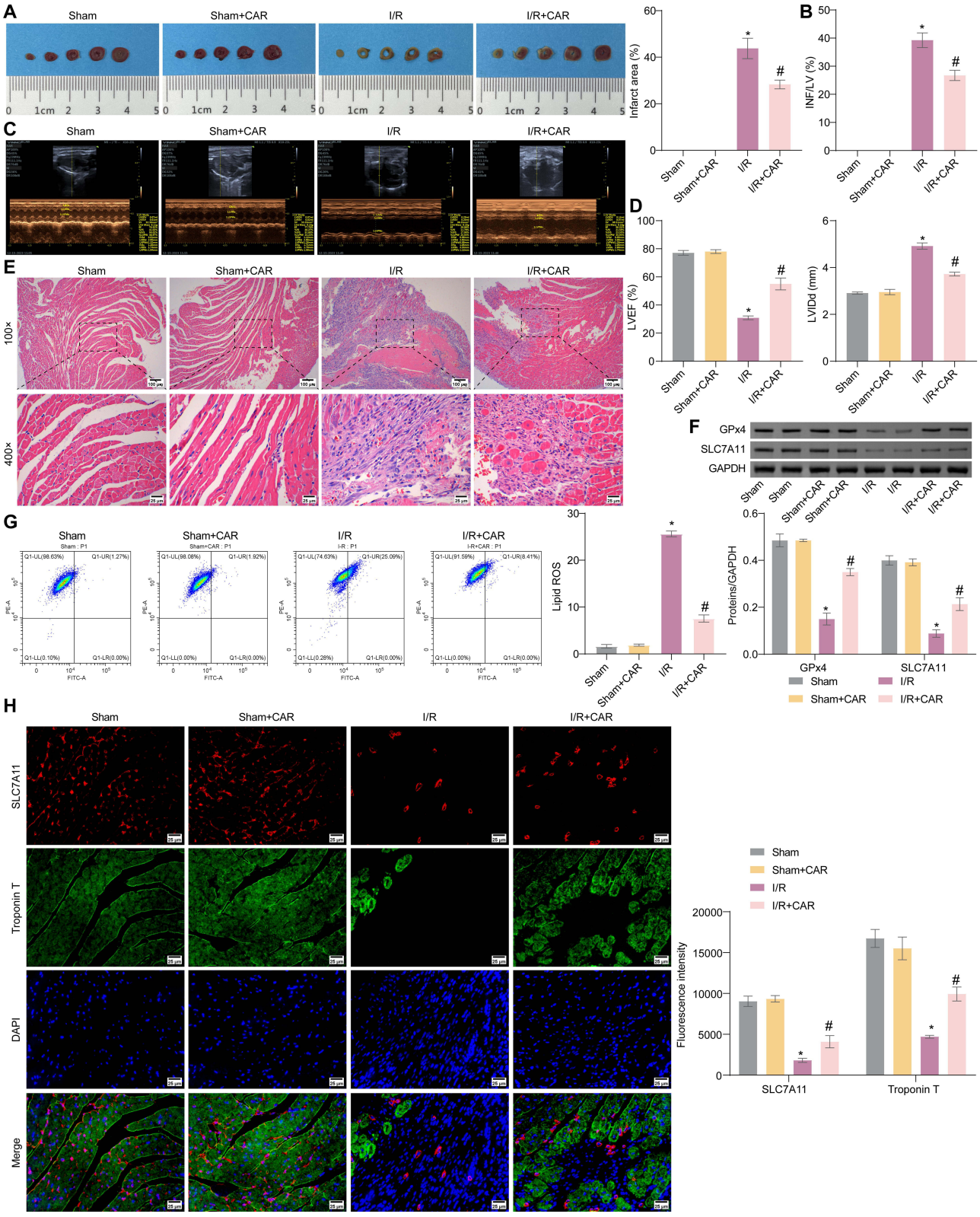

Figure 1 CAR intervention alleviates MIRI-induced ferroptosis. The MIRI model was conducted by coronary artery ligation followed by reperfusion. (**A**) The left panel displays illustrative images of myocardial tissues, while the right panel denotes the percentage of infarction size. n = 3 per group. (**B**) Measurement of the injury severity assessed through INF/LV quantification. n = 3 per group. (**C**) Illustrative echocardiograms captured at 4 h following I/R injury. (**D**) The LVEF and LVIDd were shown. n = 3 per group. (**E**) Representative images of HE staining of myocardial tissues. (**F**) The expression of GPx4 and SLC7A11 was evaluated using Western blotting. n = 6 per group. (**G**) The lipid ROS level was assessed through flow cytometry. n = 3 per group. (**H**) The left panel shows representative images of SLC7A11 staining (red) and co-staining with DAPI (blue) and troponin T (green). The right panel indicates the immunofluorescence intensity of SLC7A11 and troponin T 4 h after reperfusion. n = 3 per group. **P* < 0.05 vs Sham group. #*P* < 0.05 vs I/R group.

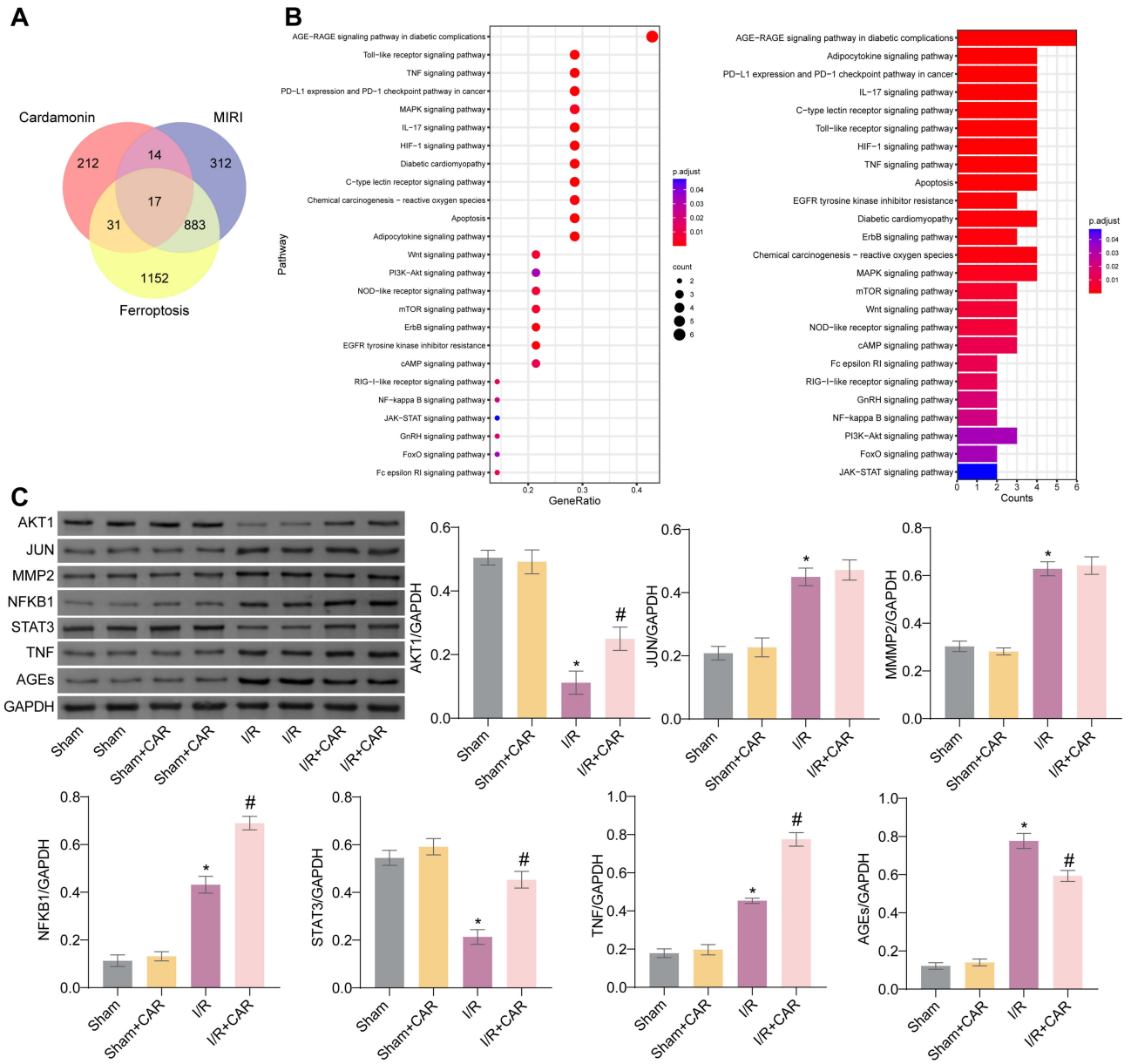

Figure 2 Network pharmacological analysis of CAR-regulated AGE-RAGE signaling pathway. (**A**) Venn analysis on putative targets of MIRI, ferroptosis, as well as CAR-related genes. (**B**) KEGG enrichment analysis of putative targets of CAR for treating MIRI. (**C**) Western blotting was performed to detect the expression levels of AGE-RAGE signaling pathway-related proteins in myocardial tissues. n = 6 per group. **P* < 0.05 vs Sham group, #*P* < 0.05 vs I/R group.

cells with BSA (as control) and different concentrations of AGEs. AGE treatment exacerbated the impaired cell viability caused by H/R in a dose-dependent manner (Figure 3A). The expression of ferroptosis-related proteins (GPx4 and SLC7A11) was then evaluated. Although there was no significant difference in GPx4 expression, the expression of SLC7A11 gradually decreased with increasing concentrations of AGEs (Figure 3B). Therefore, 150 μg/mL was chosen as the treatment concentration for AGEs in the subsequent experiments. Furthermore, to investigate whether AGEs exacerbate H/R-induced injury through ferroptosis, an intervention with Fer-1, an inhibitor of ferroptosis, was employed before H/R induction. As expected, H/R induced ferroptosis and oxidative stress in cardiomyocytes. Additionally, AGE treatment significantly further reduced the expression of SLC7A11 and elevated the lipid ROS level, while Fer-1 intervention restored them (Figure 3C and D). Iron overload is one of the key mechanisms of ferroptosis.[37] The levels of iron and ROS in mitochondria were then assessed. AGEs remarkably exacerbated the H/R-induced elevation of

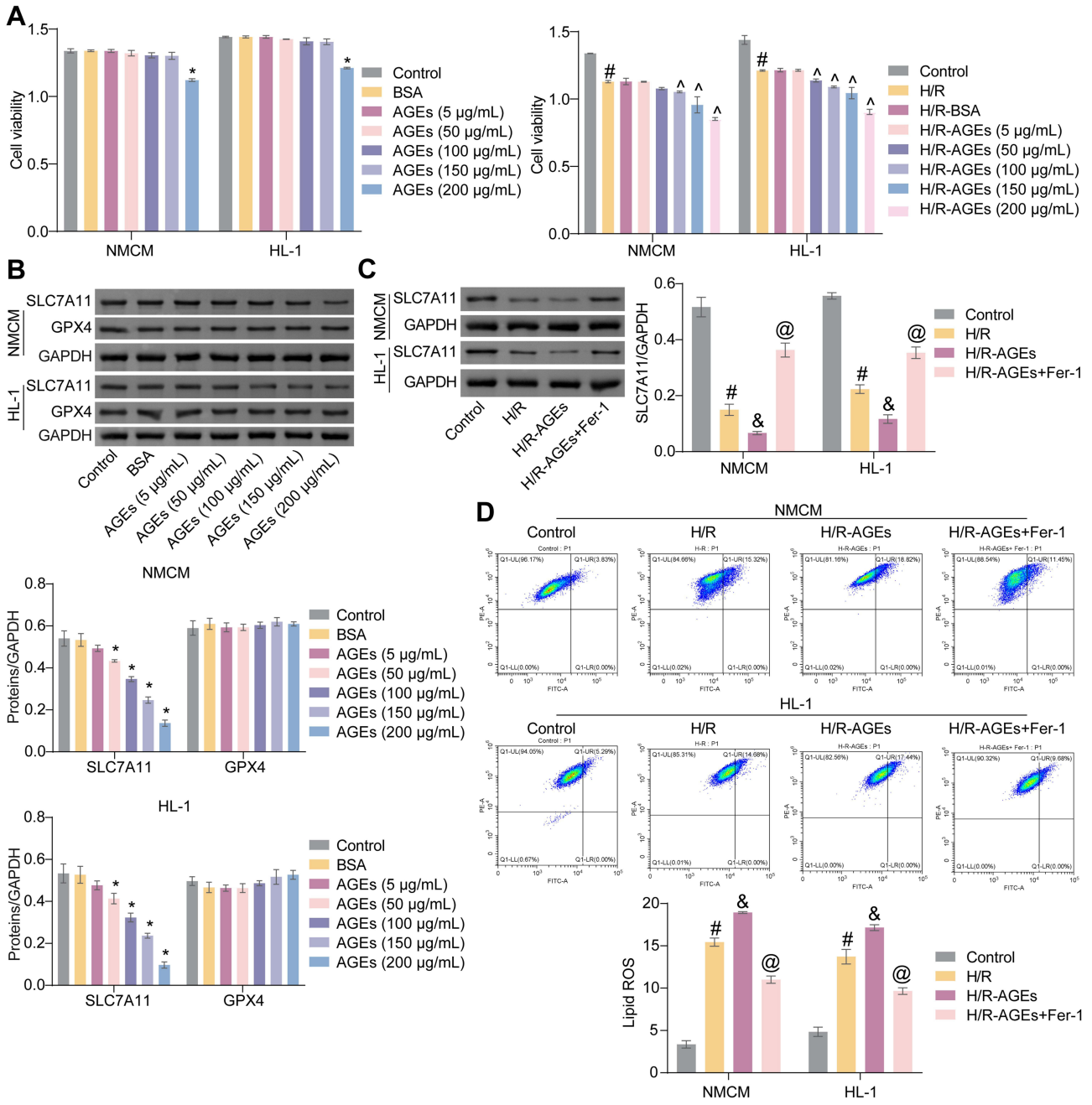

Figure 3 AGEs promote H/R-induced ferroptosis in cardiomyocytes. (**A**) The cell viability of primary cardiomyocytes and HL-1 cells was analyzed using CCK-8. (**B**) The expression levels of GPx4 and SLC7A11 were evaluated by Western blotting. (**C**) The expression of SLC7A11 was evaluated by Western blotting. (**D**) The lipid ROS level was assessed using flow cytometry. n = 3 per group. $^{*}P < 0.05$ vs BSA group, $^{\#}P < 0.05$ vs Control group, $^{\wedge}P < 0.05$ vs H/R-BSA group, $^{\&}P < 0.05$ vs H/R group, $^{@}P < 0.05$ vs H/R-AGEs group.

mitochondrial iron and ROS, which was alleviated by Fer-1 intervention (Figure 4A). As exhibited in Figure 4B, compared with the H/R group, the reduced concentration of GSH, the enhanced concentration of MDA, and the reduced activity of SOD in primary cardiomyocytes and HL-1 cells were noted in the H/R-AGEs group. In contrast, Fer-1 treatment resulted in the enhancement of GSH concentration, the reduction of MDA concentration, and the enhancement of SOD activity. Moreover, flow cytometry results show that the PI-positive cells were significantly increased after H/R treatment and AGEs further exacerbated cell death. However, compared to the H/R-AGEs group, Fer-1 treatment partly improved cell death (Figure 4C). In sum, the above data suggest that AGEs significantly promote H/R-induced oxidative stress and lipid peroxidation through ferroptosis.

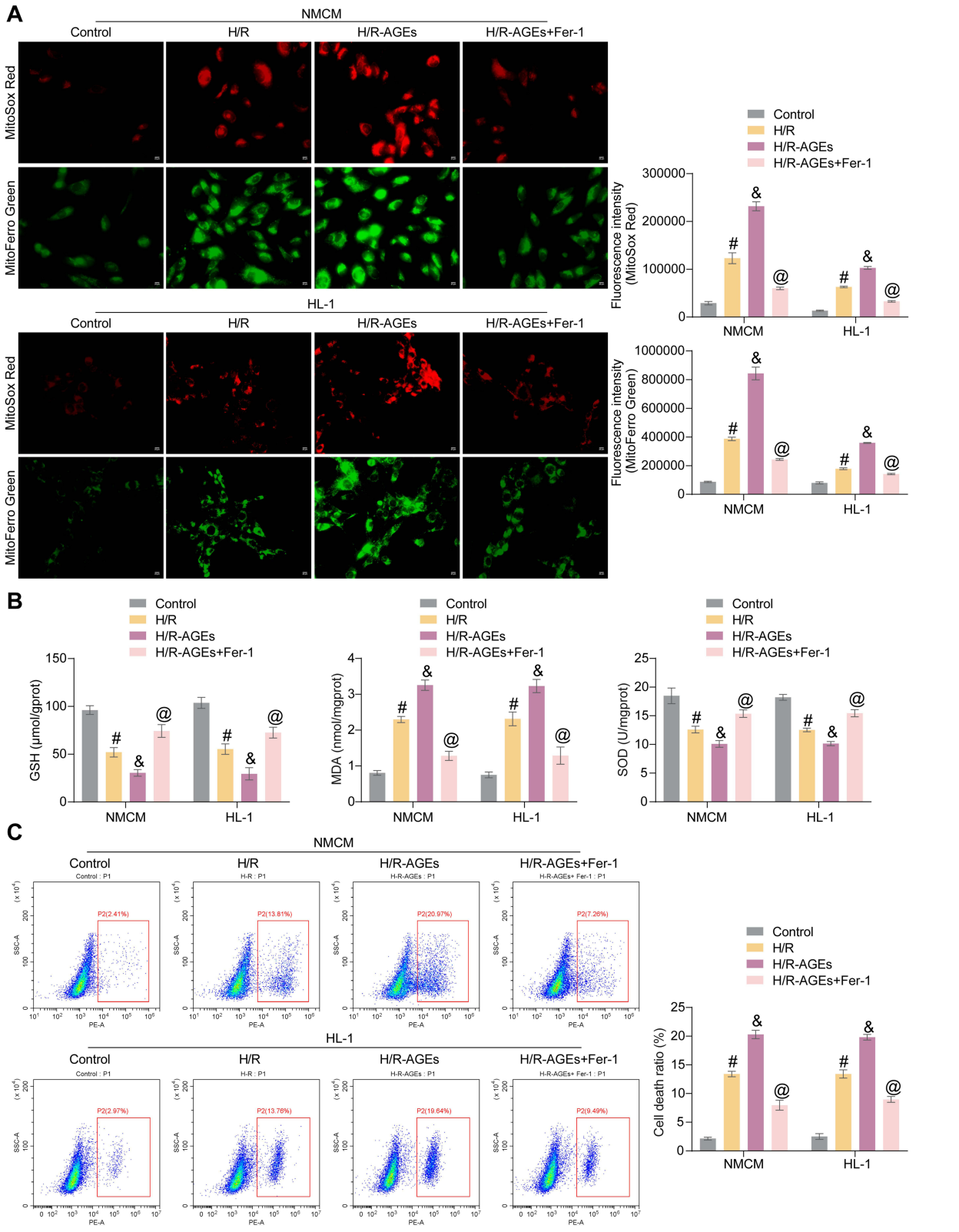

Figure 4 AGEs promote H/R-induced ferroptosis in cardiomyocytes. (**A**) The left panel shows representative images of mitochondrial iron staining (MitoFerroGreen) and mitochondrial ROS (MitoSox Red). The right panel indicates the immunofluorescence intensity of iron and ROS. (**B**) Quantification of GSH, MDA, and SOD in primary cardiomyocytes and HL-1 cells. (**C**) The ratio of cell death was assessed through flow cytometry. n = 3 per group. $^{\#}P < 0.05$ vs Control group, $^{\&}P < 0.05$ vs H/R group, $^{@}P < 0.05$ vs H/R-AGEs group.

CAR Alleviates AGE-H/R-Induced Ferroptosis Accompanied by Increased STAT3 Expression in Cardiomyocytes

Next, the role of CAR in regulating ferroptosis in cardiomyocytes in vitro was investigated. The cell viability was significantly reduced by co-treatment with H/R and AGEs, while it was restored by either CAR administration or Fer-1 intervention (Figure 5A). Moreover, the decreased SLC7A11 expression caused by H/R-AGEs was elevated after CAR or Fer-1 treatment (Figure 5B). Likewise, the levels of lipid peroxidation and oxidative stress were significantly promoted in cardiomyocytes of the H/R-AGEs group. However, these levels were inhibited when cells were treated with either CAR or Fer-1 (Figure 5C-E). In addition, according to flow cytometry results, CAR or Fer-1 intervention significantly migrated the cell death caused by H/R-AGEs (Figure 5F). These findings indicate that CAR relieves AGEs along with H/R-induced ferroptosis in cardiomyocytes.

The above network pharmacological analyses and in vivo experimental validation showed that CAR modulates the AGE-RAGE signaling pathway. Specifically, the expression of AKT1 and STAT3 was downregulated in MIRI mice, while it was restored by CAR treatment. The expression of AKT1 and STAT3 was then evaluated in vitro. Consistent with the in vivo data, the reduced expression of AKT1 and STAT3 was significantly increased by CAR, with more significant effects observed in STAT3 expression (Figure 6A). Next, a molecular modeling analysis was carried out to examine the interaction between CAR and STAT3. The docking simulation positioned CAR within the extracellular region of the 3D structure of STAT3, which was modeled based on the most suitable homologous crystal structure available in the RCSB protein database. The calculated negative free energy value (−6.9 kcal/mol) from the docking analysis supports the hypothesis that the binding of CAR to the Nucleotide-Binding site of STAT3 is a spontaneous process. The results, as depicted in Figure 6B and C, exhibit nine distinct docking positions of CAR interacting with STAT3, with all displaying negative free energy values. The conformation with the lowest energy is illustrated in Figure 6D and E. The analysis revealed that CAR is situated within the hydrophobic binding cleft (represented by gray spheres in Figure 6E), surrounded by residues at the nucleotide-binding site, including GLU-229, LYS-233, GLN-232, ARG-308, GLU-311, and ASN-315. The docking outcomes collectively suggest that CAR interacts with the nucleotide-binding site of STAT3. Collectively, the above results strongly support that CAR affects ferroptosis caused by AGE-H/R through targeting STAT3. Additionally, STAT3 has been reported to regulate SLC7A11 transcription to influence ferroptosis.[38] It is hypothesized that CAR may affect ferroptosis by targeting STAT3 to regulate SLC7A11 transcription. This suggests further analysis of the regulatory role of STAT3.

STAT3 Silencing Reverses the Inhibitory Effect of CAR on Ferroptosis in Cardiomyocytes

The findings presented above indicate that STAT3 may be the target of CAR regulation within the AGE-RAGE signaling pathway. To further explore the involvement of STAT3 in the inhibition of ferroptosis by CAR, a STAT3 silencing plasmid was constructed. Transfection efficiency analysis revealed that the introduction of STAT3 silencing plasmid led to a notable decrease in STAT3 expression level in cardiomyocytes (Figure 7A). Compared with the H/R-AGEs group, the levels of lipid ROS, mitochondrial iron, mitochondrial ROS, MDA, and cell death ratio in the H/R-AGEs+CAR group were significantly reduced and the levels of SLC7A11 expression, GSH, and SOD were significantly increased (Figure 7B-G). This implies that CAR significantly alleviated lipid peroxidation and oxidative stress injury induced by H/R and AGE co-treatment in cardiomyocytes. However, STAT3 silencing remarkably reversed the CAR regulation of these injury indicators compared to the H/R-AGEs+CAR group (Figure 7B-G). Above all, CAR exerts an inhibitory role on ferroptosis through upregulating STAT3 in cardiomyocytes.

CAR Targeting STAT3 Signaling Inhibits MIRI-Induced Ferroptosis in Mice

Given the regulatory impact of CAR on ferroptosis in vitro, we further assessed the effect of CAR on ferroptosis in the MIRI mice and verified the functional significance of the relationship between CAR and STAT3. Adenovirus targeting STAT3 was injected into the aortic root of mice five days before I/R treatment. We observed that STAT3 shRNA significantly increased infarct size, INF/LV ratio, and LVIDd when compared to the I/R+CAR+sh-NC group (Figure 8A-D). Meanwhile, the LVEF level was reduced when STAT3 was silenced (Figure 8D). Analyses of cardiomyocytes by HE staining revealed

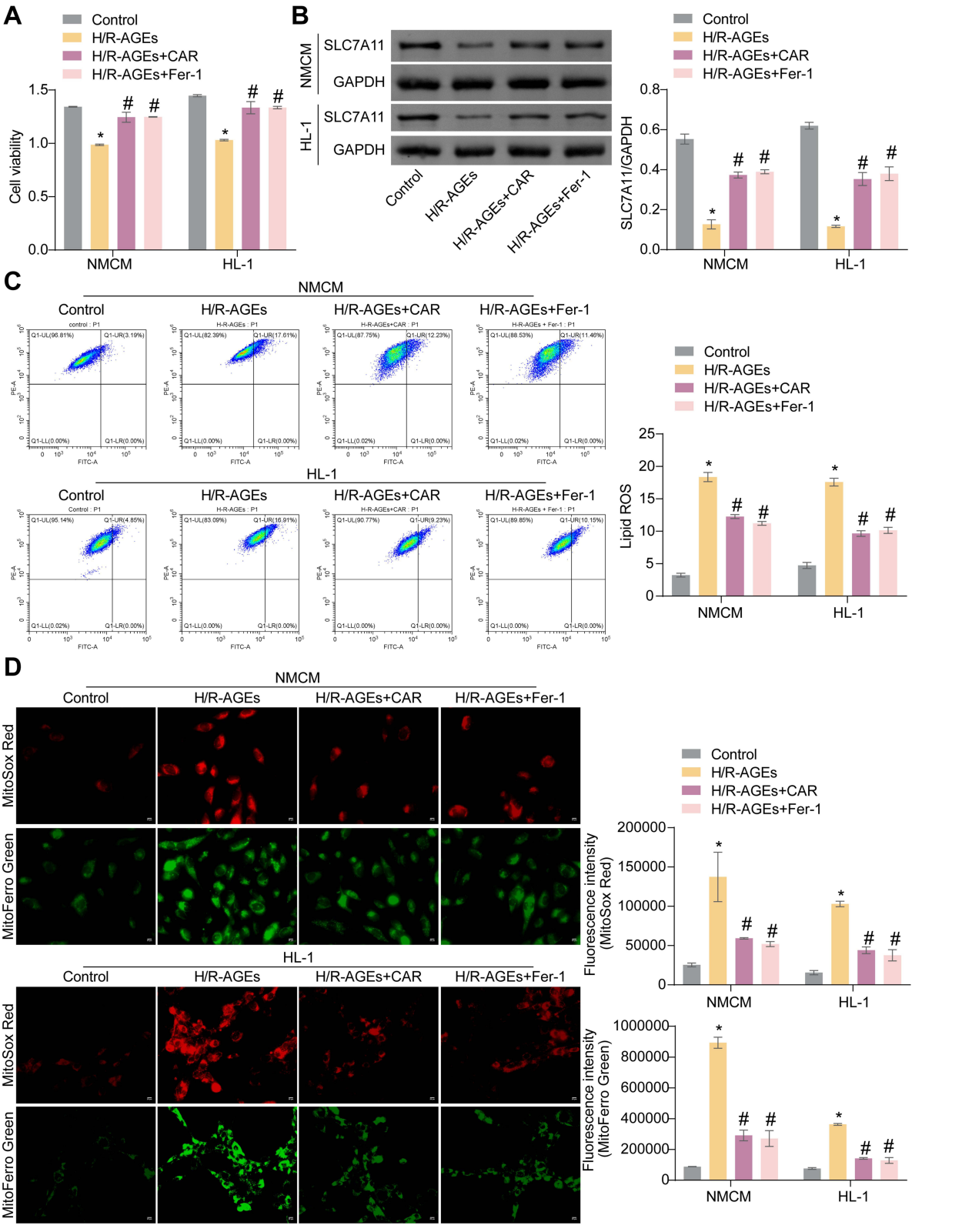

Figure 5 Continued.

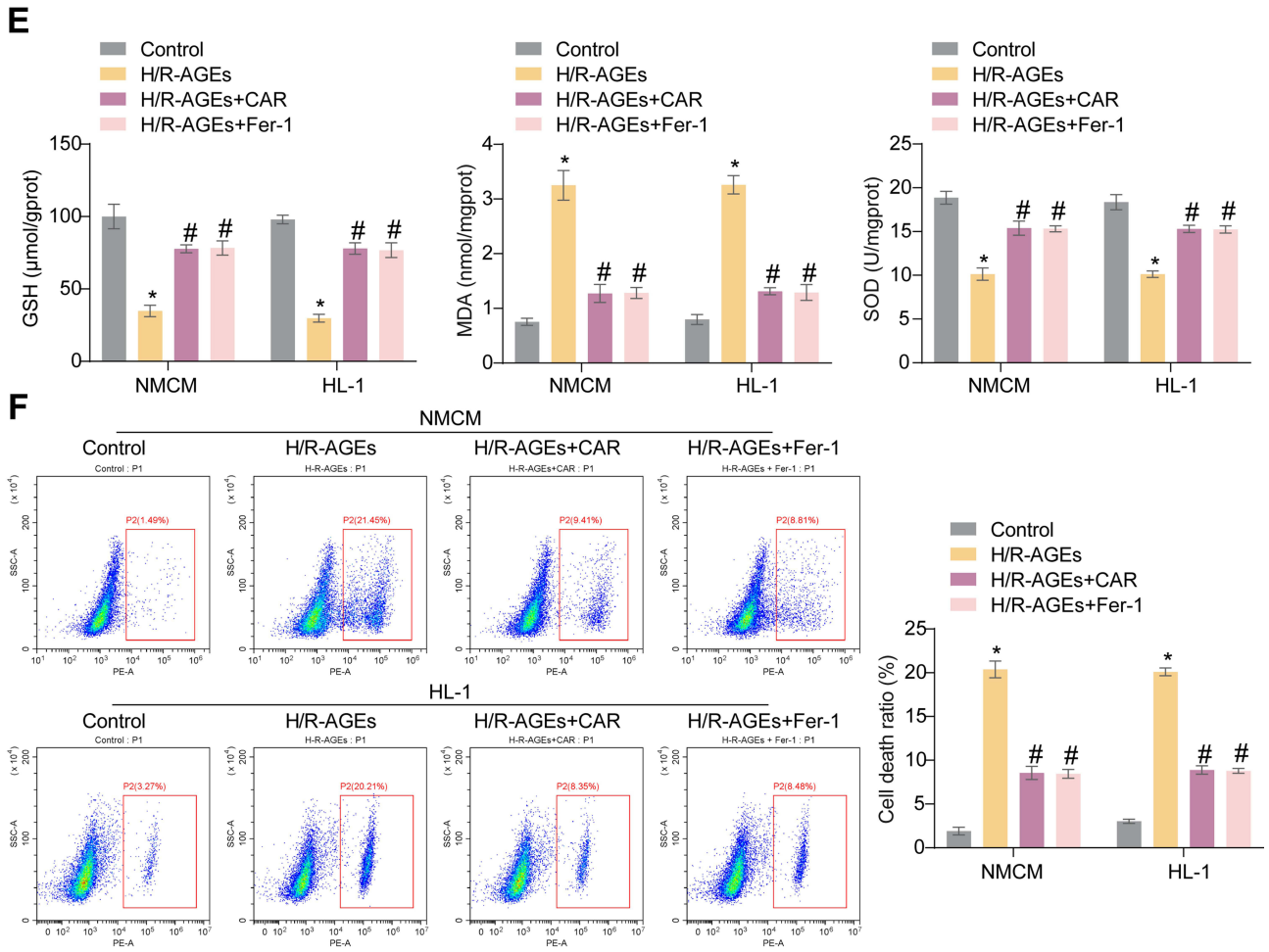

Figure 5 CAR alleviates AGE-H/R-induced ferroptosis in cardiomyocytes. (**A**) The cell viability of primary cardiomyocytes and HL-1 cells was analyzed using CCK-8. (**B**) The expression of SLC7A11 was evaluated by Western blotting. (**C**) The lipid ROS level was assessed by flow cytometry. (**D**) The left panel shows representative images of mitochondrial iron staining (MitoFerro Green) and mitochondrial ROS (MitoSox Red). The right panel indicates the immunofluorescence intensity of iron and ROS. (**E**) Quantification of GSH, MDA, and SOD in primary cardiomyocytes and HL-1 cells. (**F**) The ratio of cell death was assessed through flow cytometry. $^{*}P < 0.05$ vs Control group, $^{\#}P < 0.05$ vs H/R-AGEs group.

that STAT3 downregulation caused discontinuous tissue architecture due to extensive apoptosis (Figure 8E). These findings indicate that CAR may mitigate morphological alterations in the myocardium following I/R injury by targeting STAT3. Administering STAT3 shRNA to cardiomyocytes 4 h after I/R injury led to a significant decrease in STAT3 expression compared to sh-NC-treated mice (Figure 8F). Additionally, the impact of STAT3 knockdown on ferroptosis experiments was investigated. The expression of SLC7A11 was notably elevated and lipid ROS levels were significantly reduced under CAR treatment conditions compared to the I/R group; however, this effect was reversed by STAT3 knockdown (Figure 8F and G). In conclusion, these results suggest that CAR significantly alleviated MIRI progression through STAT3 in mice.

Discussion

I/R injury continues to be a significant issue, with the development of effective treatments for reperfusion injury still lacking. Clinical evidence indicates that during MIRI, there is a substantial generation of ROS leading to damage through lipid peroxidation.[39] CAR, also known as Alpinetin chalcone, is a naturally-occurring compound found in the fruit of Alpinia species. It has been scientifically proven to demonstrate significant anti-inflammatory and antioxidant properties in conditions such as inflammatory diseases, acute injuries, and different types of tumors.[20,23,24,40,41] Wang et al have found that CAR prevents doxorubicin-induced cardiotoxicity in mice by inhibiting oxidative stress and inflammation

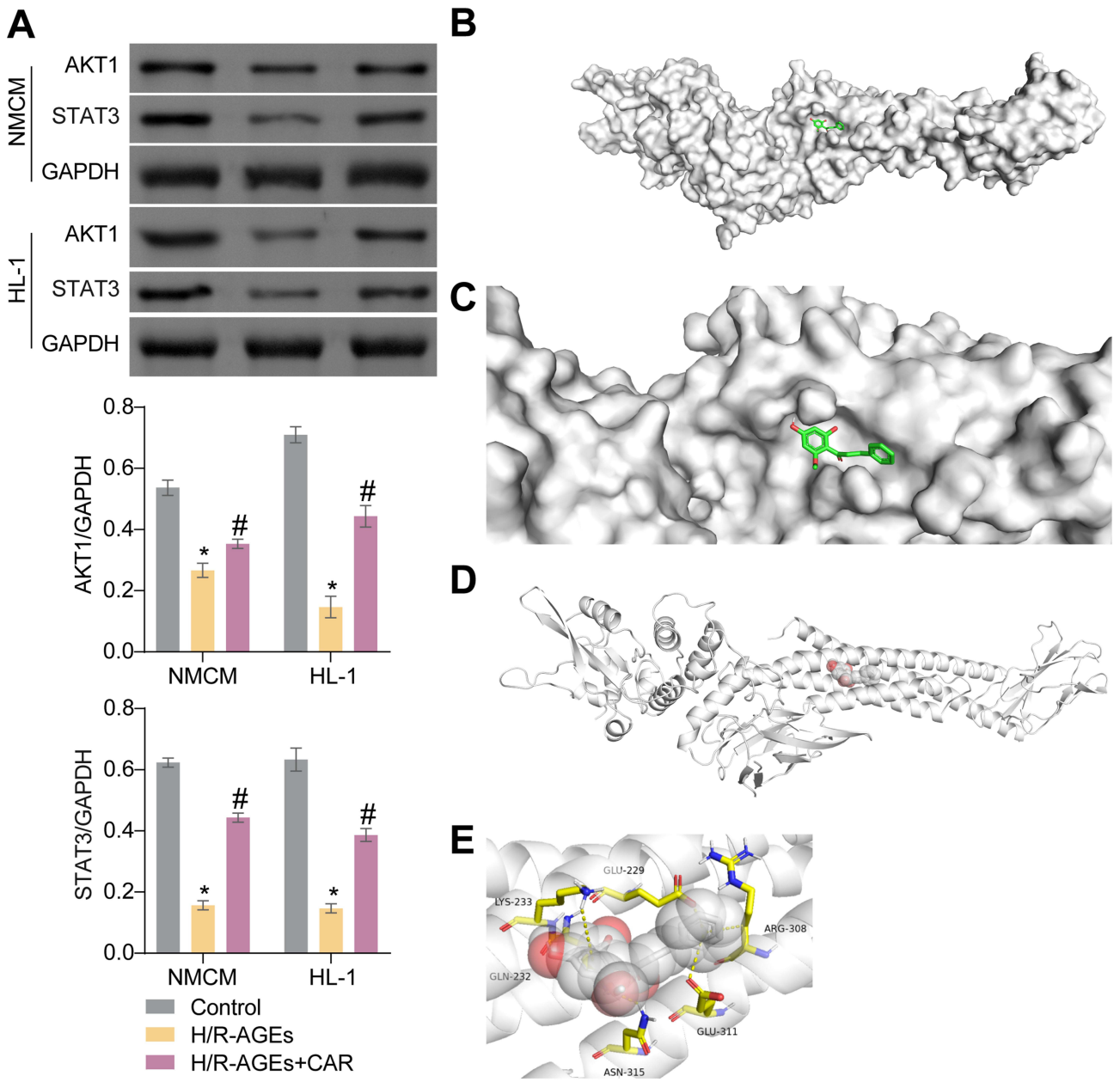

Figure 6 CAR alleviates the depression of STAT3 expression induced by AGE-H/R in cardiomyocytes. (**A**) The expression of AKT1 and STAT3 was evaluated by Western blotting. n = 3 per group. *$P < 0.05$ vs Control group, #$P < 0.05$ vs H/R-AGEs group. (**B**) Nine distinct docking positions of CAR were observed interacting with the STAT3. (**C**) Zoom view of the docking position of CAR within the nucleotide-binding domain of STAT. (**D**) The most energetically favorable conformation of CAR interacting with the STAT3 was identified. (**E**) The binding orientation and interactions of CAR with protein residues at the active site of STAT3 were investigated.

associated with Nrf2 signaling.[26] Feng et al recently reported significant mitigating effects of CAR on TAC-induced myocardial hypertrophy, fibrosis, inflammation, and oxidative stress.[28] In the present study, we established the I/R-induced cardiac injury model in vivo and used the OGDR-induced injury model in vitro to mimic the I/R injury. The protective effect of CAR was observed in both in vivo cardiac I/R injury and OGDR-treated cardiomyocytes in vitro. Similarly, CAR has been reported to alleviate I/R injury in the kidney[24] and liver.[25] Functionally, CAR significantly prevented cardiac I/R injury, as evidenced by reduced infarct size and preserved cardiac function, suggesting that CAR treatment of cardiac I/R injury is a viable therapeutic intervention. In our study, CAR was observed for the first time to attenuate I/R-induced ferroptosis in cardiomyocytes. Mechanistically, we found that CAR targeting STAT3 alleviated

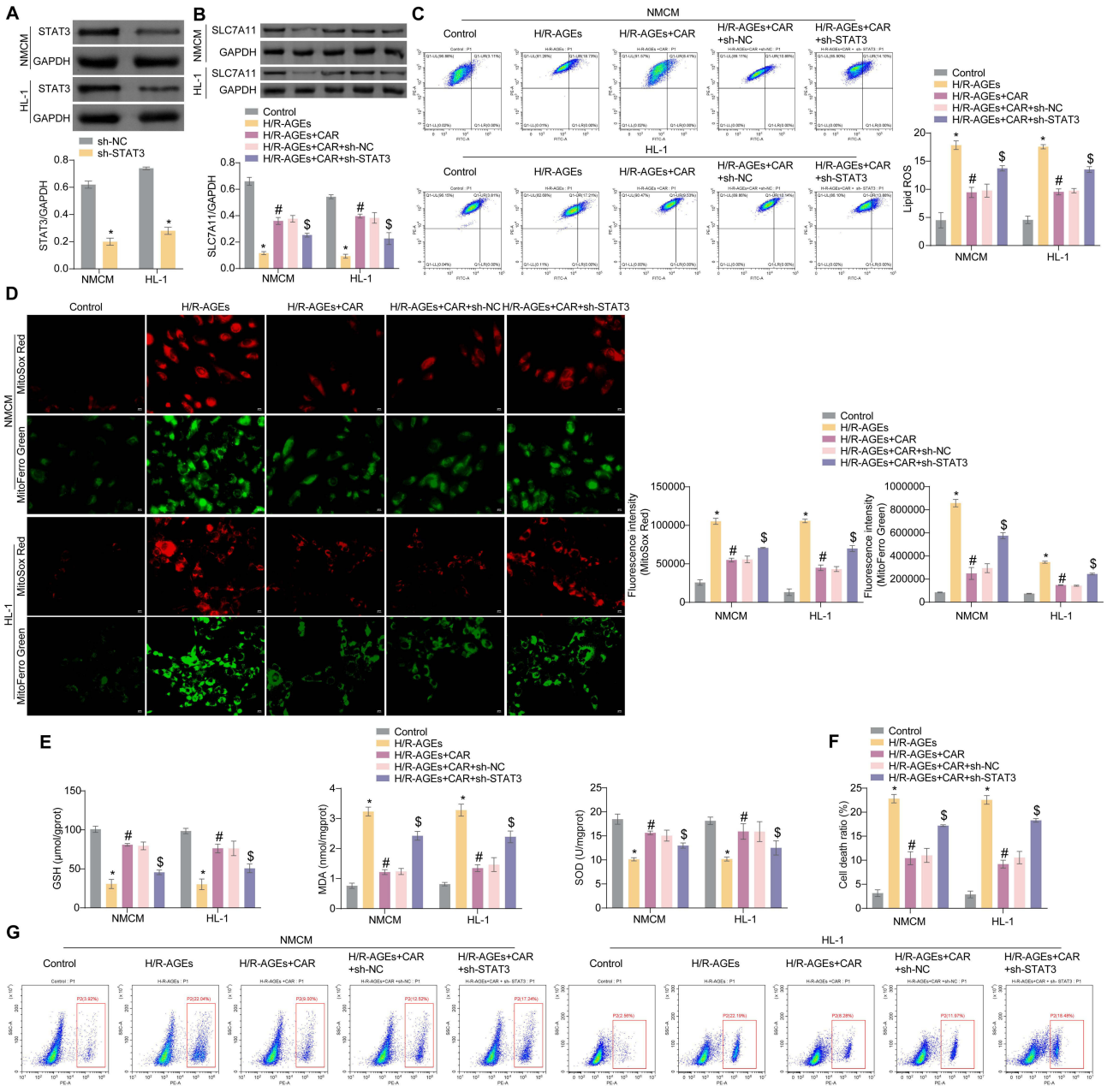

Figure 7 STAT3 silencing reverses the inhibitory effect of CAR on ferroptosis in cardiomyocytes. (**A**) The expression level of STAT3 was analyzed using Western blotting. **P* < 0.05 vs sh-NC group. (**B**) The expression of SLC7A11 was evaluated by Western blotting. (**C**) The lipid ROS level was assessed by flow cytometry. (**D**) The left panel shows representative images of mitochondrial iron staining (MitoFerro Green) and mitochondrial ROS (MitoSox Red). The right panel indicates the immunofluorescence intensity of iron and ROS. (**E**) Quantification of GSH, MDA, and SOD in primary cardiomyocytes and HL-1 cells. (**F** and **G**) The ratio of cell death was assessed through flow cytometry. n = 3 per group. **P* < 0.05 vs Control group, $^{\#}P$ < 0.05 vs H/R-AGEs group, $^{\$}P$ < 0.05 vs H/R-AGEs+CAR+sh-NC group.

HR-induced oxidative stress and cardiomyocyte injury through the AGE-RAGE signaling pathway by network pharmacological prediction and experimental validation in vivo and in vitro.

Ferroptosis is a critical pathological feature of I/R injury, which may further contribute to the development of cardiac remodeling and heart failure.[42] Disruption of the System xc^{-}/GSH/GPX4 antioxidant axis has been identified as the primary mechanism underlying ferroptosis induction, with decreased expression of key associated proteins such as SLC7A11 and GPX4 resulting in reduced cellular antioxidant capacity and subsequent ferroptosis. Previous studies based on isolated cardiac perfusion or coronary artery ligation have shown that iron chelators can attenuate cardiac injury by inhibiting ferroptosis.[13,17,43] CAR acts as an antioxidant to mitigate oxidative stress damage in various disease models.[20,44,45]

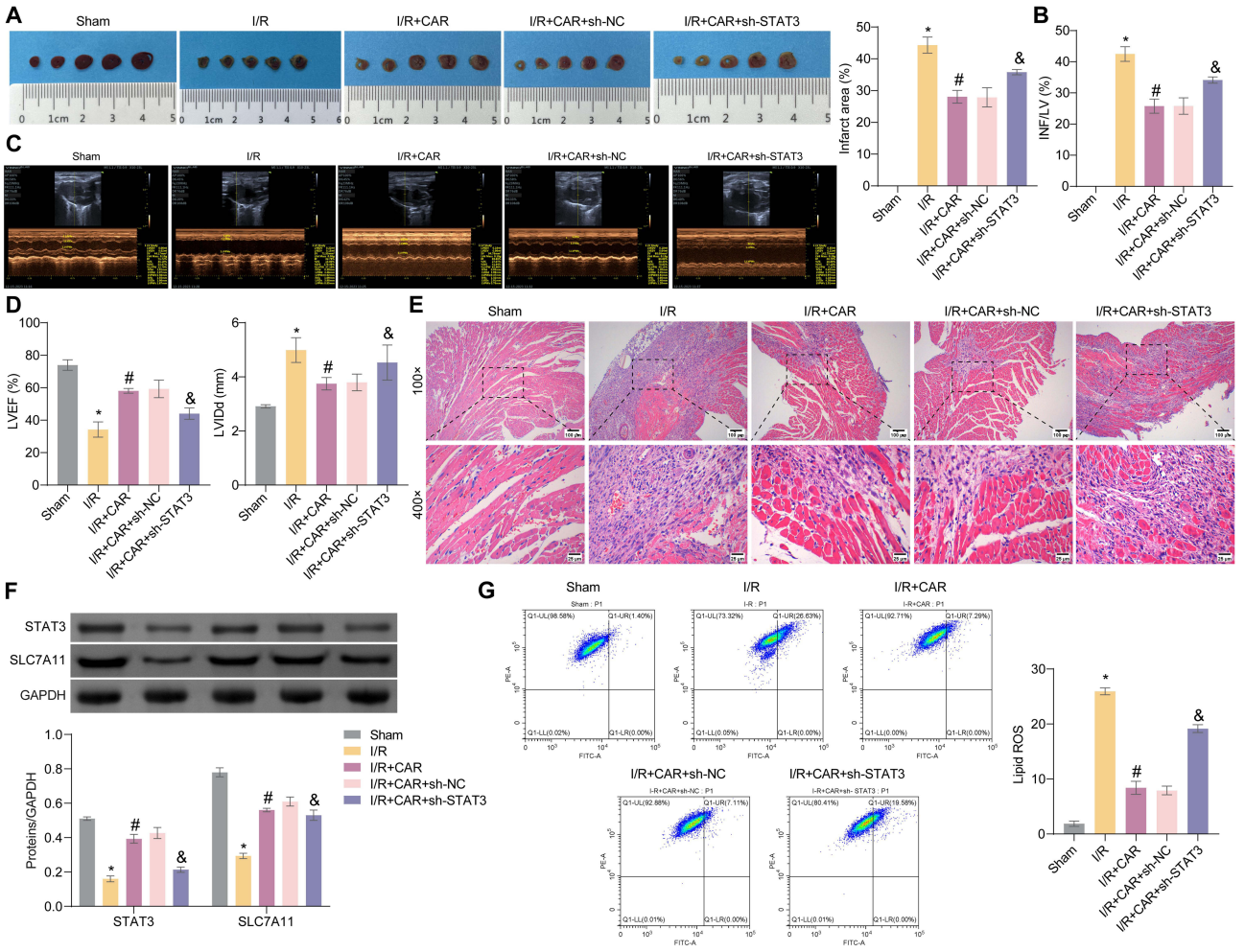

Figure 8 CAR targeting STAT3 signaling inhibits MIRI-induced ferroptosis in mice. (**A**) The left panel displays illustrative images of myocardial tissues, while the right panel denotes the percentage of infarction size. (**B**) Measurement of the injury severity assessed through INF/LV quantification. (**C**) Illustrative echocardiograms captured at 4 h following I/R injury. (**D**) The ejection fraction of the left ventricle (LVEF) and diastolic diameter of the left ventricle (LVIDd) were shown. (**E**) Representative images of HE staining of myocardial tissues. (**F**) The expression of STAT3 and SLC7A11 was evaluated using Western blotting. (**G**) The lipid ROS level was assessed through flow cytometry. n = 3 per group. $^{*}P < 0.05$ vs Sham group, $^{\#}P < 0.05$ vs I/R group, $^{\&}P < 0.05$ vs I/R+CAR+sh-NC group.

Furthermore, CAR demonstrated potent anti-inflammatory and anti-iron overload properties in an osteoporosis mouse model with intraperitoneal injection of iron dextran.[46] Gong et al have reported that CAR inhibits ferroptosis via the p53 pathway and alleviates chondrocyte inflammation and cartilage degradation in osteoarthritis.[29] In our study, it was observed that CAR significantly attenuated ferroptosis in mice with MIRI. This was evidenced by decreased levels of ROS and lipid peroxidation and increased expression of ferroptosis-related protein SLC7A11 as indicated by Western blotting and immunofluorescence analysis.

To further validate the corresponding biological processes and signaling pathways for the cardioprotective effects of CAR, we utilized network pharmacological analyses to identify that CAR modulated the AGE-RAGE signaling pathway and verified that CAR modulated the expression of AGE-RAGE signaling pathway-related proteins in I/R mice and H/R-treated cardiomyocytes by in vivo and in vitro experiments. AGEs are a diverse group of molecules resulting from nonenzymatic modifications of large molecules such as proteins, lipids, and nucleic acids by sugars like glucose, fructose, and pentose. These AGEs are considered harmful and have been observed to be elevated in the blood of individuals experiencing natural aging, age-related conditions, diabetes mellitus, and autoimmune or inflammatory rheumatic disorders such as systemic lupus erythematosus, rheumatoid arthritis, systemic sclerosis, adult-onset Still's disease, and psoriasis.[47,48] Upon binding to RAGs, the accumulation of AGEs can lead to metabolic challenges including elevated blood sugar levels (hyperglycemia) and high levels of fats in the blood (hyperlipidemia), as well as oxidative stress,

inflammatory reactions, and impaired function of the endothelium.[49,50] Liu et al found that AGEs accelerate I/R injury via receptor of advanced end product/nitrative thioredoxin inactivation in cardiac microvascular endothelial cells.[36] AGEs are also capable of inducing ferroptosis in diabetic cardiomyopathy.[33] Similarly, in our study, we found that AGE intervention significantly promoted H/R-induced cardiomyocyte ferroptosis. In an in vitro model using primary mouse cardiomyocytes and HL-1 cells subjected to H/R, treatment with AGEs significantly increased myocardial iron and ROS accumulation and levels of MDA, lipid ROS, and PI-positive ratio, while SLC7A11 expression, GSH level, and SOD activity were notably reduced. Administration of ferroptosis inhibiter Fer-1 to H/R model cells treated with AGEs resulted in a marked decrease in iron accumulation and lipid peroxidation levels, indicating that AGEs may protect cardiomyocyte cells from H/R-induced damage by inhibiting ferroptosis.

Furthermore, in our study, through evaluation of the expression levels of the AGE-RAGE signaling pathway in mouse myocardial tissues and cardiomyocytes, we found the most significant differences in STAT3. The STAT3 protein is responsible for regulating the expression of numerous genes in reaction to cellular signals, thereby influencing essential cellular functions like cell proliferation and programmed cell death.[51] Zhao et al demonstrated that cardiomyocyte LGR6 alleviates ferroptosis in diabetic cardiomyopathy through the regulation of STAT3/Pgc1a signaling.[52] A previous study has documented that STAT3 regulated SLC7A11 transcription to affect ferroptosis.[38] In our study, molecular docking of CAR and STAT3 showed a binding energy of −6.9 kcal/mol, implying that these two molecules are capable of spontaneous binding. In addition, the study also investigated the role of STAT3 in regulating ferroptosis during MIRI in mice by administering the STAT3 shRNA, which resulted in significantly increased myocardial histopathological damage, iron accumulation, and lipid peroxidation. This suggests that CAR may ameliorate MIRI in mice by activating STAT3 and thereby inhibiting ferroptosis. Comparably, CAR was also able to significantly inhibit STAT3 activation in a variety of tumor cells.[41,53,54]

The following limitations should be considered when interpreting our findings. The impact of MIRI extends beyond cardiomyocyte death to various cell types such as platelets, fibroblasts, endothelial and smooth muscle cells, and immune cells, which could potentially contribute to the cardioprotective effects of CAR.[55] While our current investigation is confined to cardiomyocytes and does not delve into the influence of CAR on other cell types, it is essential to note that the applicability of our findings to clinical settings necessitates further validation through clinical trials. Therefore, additional research is imperative to confirm the relationship between the cardioprotective properties of CAR and its ability to resist ferroptosis.

Conclusion

In this investigation, it was demonstrated that the STAT3 and AGE-RAGE signaling pathway potentially play a role in facilitating the cardioprotective effects of CAR in mice subjected to MIRI. CAR targeting STAT3 signaling inhibits MIRI-induced ferroptosis. This research offers valuable insights and a scientific foundation for further exploration of the mechanistic and therapeutic aspects of MIRI in clinical settings.

Acknowledgments

We thank all the staff of The Affiliated Changsha Central Hospital, Hengyang Medical School, University of South China for their support of our research.

Funding

This study was supported by the Changsha Municipal Natural Science Foundation (Nos. kq2202048, kq2403164, kq2403165), the Scientific Research Project of Hunan Provincial Health Commission (No. B202303016247), the Scientific Research Project of Changsha Municipal Health Commission (No. KJ-B2023028).

Disclosure

The author(s) report no conflicts of interest in this work.

References

1. Li J, Miao B, Wang S, et al. Hiplot: a comprehensive and easy-to-use web service for boosting publication-ready biomedical data visualization. *Brief Bioinform*. 2022;23(4). doi:10.1093/bib/bbac261

2. Asaria P, Bennett JE, Elliott P, et al. Contributions of event rates, pre-hospital deaths, and deaths following hospitalisation to variations in myocardial infarction mortality in 326 districts in England: a spatial analysis of linked hospitalisation and mortality data. *Lancet Public Health*. 2022;7(10):e813–e824. doi:10.1016/s2468-2667(22)00108-6
3. Yellon DM, Hausenloy DJ. Myocardial reperfusion injury. *N Engl J Med*. 2007;357(11):1121–1135. doi:10.1056/NEJMra071667
4. Hausenloy DJ, Yellon DM. Targeting myocardial reperfusion injury–the search continues. *N Engl J Med*. 2015;373(11):1073–1075. doi:10.1056/NEJMe1509718
5. He J, Liu D, Zhao L, et al. Myocardial ischemia/reperfusion injury: mechanisms of injury and implications for management (Review). *Exp Ther Med*. 2022;23(6):430. doi:10.3892/etm.2022.11357
6. Xiang Q, Yi X, Zhu XH, Wei X, Jiang DS. Regulated cell death in myocardial ischemia-reperfusion injury. *Trends Endocrinol Metab*. 2024;35(3):219–234. doi:10.1016/j.tem.2023.10.010
7. Li J, Zhang J, Zhong Y, et al. TRPC6 regulates necroptosis in myocardial ischemia/reperfusion injury via Ca(2+)/CaMKII signaling pathway. *Cell Signal*. 2024;122:111344. doi:10.1016/j.cellsig.2024.111344
8. Zhu K, Fan R, Cao Y, et al. Glycyrrhizin attenuates myocardial ischemia reperfusion injury by suppressing Inflammation, oxidative stress, and ferroptosis via the HMGB1-TLR4-GPX4 pathway. *Exp Cell Res*. 2024;435(1):113912. doi:10.1016/j.yexcr.2024.113912
9. Dixon SJ, Lemberg KM, Lamprecht MR, et al. Ferroptosis: an iron-dependent form of nonapoptotic cell death. *Cell*. 2012;149(5):1060–1072. doi:10.1016/j.cell.2012.03.042
10. Fang X, Ardehali H, Min J, Wang F. The molecular and metabolic landscape of iron and ferroptosis in cardiovascular disease. *Nat Rev Cardiol*. 2023;20(1):7–23. doi:10.1038/s41569-022-00735-4
11. Ju J, Song YN, Wang K. Mechanism of ferroptosis: a potential target for cardiovascular diseases treatment. *Aging Dis*. 2021;12(1):261–276. doi:10.14336/ad.2020.0323
12. Zhang CH, Yan YJ, Luo Q. The molecular mechanisms and potential drug targets of ferroptosis in myocardial ischemia-reperfusion injury. *Life Sci*. 2024;340:122439. doi:10.1016/j.lfs.2024.122439
13. Fang X, Wang H, Han D, et al. Ferroptosis as a target for protection against cardiomyopathy. *Proc Natl Acad Sci*. 2019;116(7):2672–2680. doi:10.1073/pnas.1821022116
14. Miyamoto HD, Ikeda M, Ide T, et al. Iron overload via heme degradation in the endoplasmic reticulum triggers ferroptosis in myocardial ischemia-reperfusion injury. *JACC Basic Transl Sci*. 2022;7(8):800–819. doi:10.1016/j.jacbts.2022.03.012
15. Cai W, Liu L, Shi X, et al. Alox15/15-HpETE aggravates myocardial ischemia-reperfusion injury by promoting cardiomyocyte ferroptosis. *Circulation*. 2023;147(19):1444–1460. doi:10.1161/circulationaha.122.060257
16. Zhang AY, Su JB, Sun HT, et al. Stachyose ameliorates myocardial ischemia-reperfusion injury by inhibiting cardiomyocyte ferroptosis and macrophage pyroptosis. *Int Immunopharmacol*. 2024;143(Pt 1):113334. doi:10.1016/j.intimp.2024.113334
17. Li W, Feng G, Gauthier JM, et al. Ferroptotic cell death and TLR4/Trif signaling initiate neutrophil recruitment after heart transplantation. *J Clin Invest*. 2019;129(6):2293–2304. doi:10.1172/jci126428
18. Wu A, Zhong C, Song X, et al. The activation of LBH-CRYAB signaling promotes cardiac protection against I/R injury by inhibiting apoptosis and ferroptosis. *iScience*. 2024;27(5):109510. doi:10.1016/j.isci.2024.109510
19. Ju J, Li XM, Zhao XM, et al. Circular RNA FEACR inhibits ferroptosis and alleviates myocardial ischemia/reperfusion injury by interacting with NAMPT. *J Biomed Sci*. 2023;30(1):45. doi:10.1186/s12929-023-00927-1
20. Peng YJ, Lu JW, Lee CH, et al. Cardamonin attenuates inflammation and oxidative stress in interleukin-1β-stimulated osteoarthritis chondrocyte through the Nrf2 pathway. *Antioxidants*. 2021;10(6). doi:10.3390/antiox10060862
21. Nawaz J, Rasul A, Shah MA, et al. Cardamonin: a new player to fight cancer via multiple cancer signaling pathways. *Life Sci*. 2020;250:117591. doi:10.1016/j.lfs.2020.117591
22. Daimary UD, Parama D, Rana V, et al. Emerging roles of cardamonin, a multitargeted nutraceutical in the prevention and treatment of chronic diseases. *Curr Res Pharmacol Drug Discov*. 2021;2:100008. doi:10.1016/j.crphar.2020.100008
23. Ni H, Li J, Zheng J, Zhou B. Cardamonin attenuates cerebral ischemia/reperfusion injury by activating the HIF-1α/VEGFA pathway. *Phytother Res*. 2022;36(4):1736–1747. doi:10.1002/ptr.7409
24. Zhang B, Chen ZY, Jiang Z, Huang S, Liu XH, Wang L. Nephroprotective effects of cardamonin on renal ischemia reperfusion injury/UUO-induced renal fibrosis. *J Agric Food Chem*. 2023;71(36):13284–13303. doi:10.1021/acs.jafc.3c01880
25. Atef Y, El-Fayoumi HM, Abdel-Mottaleb Y, Mahmoud MF. Effect of cardamonin on hepatic ischemia reperfusion induced in rats: role of nitric oxide. *Eur J Pharmacol*. 2017;815:446–453. doi:10.1016/j.ejphar.2017.09.037
26. Qi W, Boliang W, Xiaoxi T, Guoqiang F, Jianbo X, Gang W. Cardamonin protects against doxorubicin-induced cardiotoxicity in mice by restraining oxidative stress and inflammation associated with Nrf2 signaling. *Biomed Pharmacother*. 2020;122:109547. doi:10.1016/j.biopha.2019.109547
27. Tan Y, Wan HH, Sun MM, et al. Cardamonin protects against lipopolysaccharide-induced myocardial contractile dysfunction in mice through Nrf2-regulated mechanism. *Acta Pharmacol Sin*. 2021;42(3):404–413. doi:10.1038/s41401-020-0397-3
28. Feng Z, Pan L, Qiao C, Yang Y, Yang X, Xie Y. Cardamonin intervenes in myocardial hypertrophy progression by regulating Usp18. *Phytomedicine*. 2024;134:155970. doi:10.1016/j.phymed.2024.155970
29. Gong Z, Wang Y, Li L, Li X, Qiu B, Hu Y. Cardamonin alleviates chondrocytes inflammation and cartilage degradation of osteoarthritis by inhibiting ferroptosis via p53 pathway. *Food Chem Toxicol*. 2023;174:113644. doi:10.1016/j.fct.2023.113644
30. Wu F, Huang W, Tan Q, et al. ZFP36L2 regulates myocardial ischemia/reperfusion injury and attenuates mitochondrial fusion and fission by LncRNA PVT1. *Cell Death Dis*. 2021;12(6):614. doi:10.1038/s41419-021-03876-5
31. Shao CJ, Zhou HL, Gao XZ, Xu CF. Downregulation of miR-221-3p promotes the ferroptosis in gastric cancer cells via upregulation of ATF3 to mediate the transcription inhibition of GPX4 and HRD1. *Transl Oncol*. 2023;32:101649. doi:10.1016/j.tranon.2023.101649
32. Wang Z, Yao M, Jiang L, et al. Dexmedetomidine attenuates myocardial ischemia/reperfusion-induced ferroptosis via AMPK/GSK-3β/Nrf2 axis. *Biomed Pharmacother*. 2022;154:113572. doi:10.1016/j.biopha.2022.113572
33. Wang X, Chen X, Zhou W, et al. Ferroptosis is essential for diabetic cardiomyopathy and is prevented by sulforaphane via AMPK/NRF2 pathways. *Acta Pharm Sin B*. 2022;12(2):708–722. doi:10.1016/j.apsb.2021.10.005
34. Li Y, Huang Z, Pan S, et al. Resveratrol alleviates diabetic periodontitis-induced alveolar osteocyte ferroptosis possibly via regulation of SLC7A11/GPX4. *Nutrients*. 2023;15(9). doi:10.3390/nu15092115

35. Chen X, Li J, Kang R, Klionsky DJ, Tang D. Ferroptosis: machinery and regulation. *Autophagy*. 2021;17(9):2054–2081. doi:10.1080/15548627.2020.1810918
36. Liu Y, Ma Y, Wang R, et al. Advanced glycation end products accelerate ischemia/reperfusion injury through receptor of advanced end product/nitrative thioredoxin inactivation in cardiac microvascular endothelial cells. *Antioxid Redox Signal*. 2011;15(7):1769–1778. doi:10.1089/ars.2010.3764
37. Huo C, Li G, Hu Y, Sun H. The impacts of iron overload and ferroptosis on intestinal mucosal homeostasis and inflammation. *Int J Mol Sci*. 2022;23(22):14195. doi:10.3390/ijms232214195
38. Ouyang S, Li H, Lou L, et al. Inhibition of STAT3-ferroptosis negative regulatory axis suppresses tumor growth and alleviates chemoresistance in gastric cancer. *Redox Biol*. 2022;52:102317. doi:10.1016/j.redox.2022.102317
39. Tingberg E, Ohlin AK, Gottsäter A, Ohlin H. Lipid peroxidation is not increased in heart failure patients on modern pharmacological therapy. *Int J Cardiol*. 2006;112(3):275–281. doi:10.1016/j.ijcard.2005.09.004
40. Jin J, Qiu S, Wang P, et al. Cardamonin inhibits breast cancer growth by repressing HIF-1α-dependent metabolic reprogramming. *J Exp Clin Cancer Res*. 2019;38(1):377. doi:10.1186/s13046-019-1351-4
41. Chen H, Huang S, Niu P, et al. Cardamonin suppresses pro-tumor function of macrophages by decreasing M2 polarization on ovarian cancer cells via mTOR inhibition. *Mol Ther Oncolytics*. 2022;26:175–188. doi:10.1016/j.omto.2022.06.009
42. Li X, Ma N, Xu J, et al. Targeting ferroptosis: pathological mechanism and treatment of ischemia-reperfusion injury. *Oxid Med Cell Longev*. 2021;2021(1):1587922. doi:10.1155/2021/1587922
43. Fang X, Cai Z, Wang H, et al. Loss of cardiac ferritin h facilitates cardiomyopathy via Slc7a11-mediated ferroptosis. *Circ Res*. 2020;127(4):486–501. doi:10.1161/circresaha.120.316509
44. Li W, Wu X, Li M, et al. Cardamonin alleviates pressure overload-induced cardiac remodeling and dysfunction through inhibition of oxidative stress. *J Cardiovasc Pharmacol*. 2016;68(6):441–451. doi:10.1097/fjc.0000000000000430
45. Fan P, Meng H, Hao W, et al. Cardamonin targets KEAP1/NRF2 signaling for protection against atherosclerosis. *Food Funct*. 2023;14(10):4905–4920. doi:10.1039/d3fo00967j
46. Chen C, Chen B, Lin Y, et al. Cardamonin attenuates iron overload-induced osteoblast oxidative stress through the HIF-1α/ROS pathway. *Int Immunopharmacol*. 2024;142(Pt A):112893. doi:10.1016/j.intimp.2024.112893
47. Shen CY, Lu CH, Wu CH, et al. The development of maillard reaction, and advanced glycation end product (AGE)-receptor for AGE (RAGE) signaling inhibitors as novel therapeutic strategies for patients with AGE-related diseases. *Molecules*. 2020;25(23):5591. doi:10.3390/molecules25235591
48. Zhu J, Wang Z, Lv C, Li M, Wang K, Chen Z. Advanced glycation end products and health: a systematic review. *Ann Biomed Eng*. 2024. doi:10.1007/s10439-024-03499-9
49. Del Turco S, Basta G. An update on advanced glycation endproducts and atherosclerosis. *Biofactors*. 2012;38(4):266–274. doi:10.1002/biof.1018
50. Mori Y, Terasaki M, Osaka N, et al. DNA aptamer raised against advanced glycation end products improves sperm concentration, motility, and viability by suppressing receptors for advanced glycation end product-induced oxidative stress and inflammation in the testes of diabetic mice. *Int J Mol Sci*. 2024;25(11):5947. doi:10.3390/ijms25115947
51. Butturini E, Carcereri de Prati A, Mariotto S. Redox Regulation of STAT1 and STAT3 Signaling. *Int J Mol Sci*. 2020;21(19):7034. doi:10.3390/ijms21197034
52. Zhao M, Shen Z, Zheng Z, et al. Cardiomyocyte LGR6 alleviates ferroptosis in diabetic cardiomyopathy via regulating mitochondrial biogenesis. *Metabolism*. 2024;159:155979. doi:10.1016/j.metabol.2024.155979
53. Wang Z, Tang X, Wu X, et al. Cardamonin exerts anti-gastric cancer activity via inhibiting LncRNA-PVT1-STAT3 axis. *Biosci Rep*. 2019;39(5). doi:10.1042/bsr20190357
54. Zhang J, Sikka S, Siveen KS, et al. Cardamonin represses proliferation, invasion, and causes apoptosis through the modulation of signal transducer and activator of transcription 3 pathway in prostate cancer. *Apoptosis*. 2017;22(1):158–168. doi:10.1007/s10495-016-1313-7
55. Davidson SM, Ferdinandy P, Andreadou I, et al. Multitarget strategies to reduce myocardial ischemia/reperfusion injury: JACC review topic of the week. *J Am Coll Cardiol*. 2019;73(1):89–99. doi:10.1016/j.jacc.2018.09.086